# Investigating the dynamic movement of liquid droplets on a moving plane

Li Xin Rui (4i213), Lee Jia Jun Darius (4i212), Teh Guang Yu (4i222)

1-05

**Abstract**

In this paper, a systematic study was conducted to explore the dynamic movement of falling liquid droplets on a moving surface. Drops of liquids with varying viscosities (0.602 and 0.445 $m$ Pa $s^{-1}$) and surface tension (83.5 and 41.3 **m**$N\ m^{-1}$) were used. [1]Wide ranges of drop velocity and surface velocity were studied. High speed imaging from the side was employed to capture the behaviour of water droplets. 4 different regimes were observed, namely no bounce, semi bounce, bounce and break up. It was found that at higher velocity ($20{\sim}40\ m\ s^{-1}$), the droplet is more likely to have a complete rebound, and as height of the water droplet release is above a certain mark, at $\sim 0.85\ m$, the boundary between break up and no bounce regime decreases. Both values were lower for water with surfactant ($12{\sim}30\ m\ s^{-1}$ and $\sim 0.67\ m$ respectively) , possibly due to its higher surface tension and viscosity.

## 1. Introduction

The importance of droplet impact dynamics in a multitude of industrial applications such as inkjet printing, spray coating and the optimisation of combustion engines (Moghtadernejad, Lee & Jadidi, 2020) has driven numerous studies in this area. This paper focused on the dynamic movement of droplets on a moving surface, which is of surprising importance in applications such as the prevention of aircraft icing. Aircraft icing refers to a phenomenon where supercooled droplets track through the airflow and impact the aircraft surface, where the low energy droplets freeze upon impact (Bragg, 1996). Ice accretion on aircrafts alters the pressure distribution about the airfoil and causes premature airfoil stall. This reduction in aerodynamics of the wings increases fuel consumption. Thus, a detailed understanding of droplet behaviour when impacting a mobile surface is much needed in the optimisation of aircraft wings (Wu, 2018) and other industrial processes.

It has been observed that a drop hitting a solid surface can deposit, bounce or splash (Andrede et al., 2013; Bird et al., 2013). However, when the surface is moving at a certain velocity, and the drop is released right above the surface, it can be observed to be levitating.

[1] **m** refers to milli ($10^{-3}$) while $m$ refers to metre.

This phenomenon was observed by Sawaguchi et al. (2018). Lhussier et al. (2013) proposes an interesting mechanism behind this phenomenon, where pressure build-up generated by the lubrication flow under the drop generates sufficient lift to prevent contact of the drop and the surface. Gauthier et al. (2018) found that a variation of this reaction can be seen when the drop velocity is greater than zero, with his observation that impacting liquids can be repelled by moving solid plates, provided the surface is moving at a high enough velocity. It has been observed that there exists a boundary layer of air under the droplet which exerts dynamic pressure on the drop, generating the necessary lift for drop rebound (Bouwhis, 2015; Chubynsky et al., 2020).

In order to further investigate the hydrophobic-like behaviour of drops on a moving surface, a simple experimental setup is presented, allowing the simulation of a steady moving surface. The setup features a rotating acrylic disk coupled with high-speed imaging to observe the behaviour of the drops and was inspired by a similar configuration used by Povarov et al. (1976) to study the drop trajectory of repelling liquid released from an overhanging syringe. Further tests were carried out to observe the effects of drop velocity, drop viscosity and surface velocity, which would be discussed in the latter part of this paper.

## 2. Objectives and hypotheses

### 2.1 Rationale

This project aims to explore the hydrophobic-like behaviour of liquid on a moving surface, which can help optimise the inkjet printer, aircraft efficiency and other areas where applicable.

### 2.2 Hypothesis

1. Above a certain surface speed, the liquid droplet will be repelled off the moving surface.
2. At higher impact velocity of droplets, lower surface speed is required for drop rebound.
3. At greater viscosities of liquid, higher surface speed is needed for drop rebound.

## 3. Methods and Materials

### 3.1 Materials

A piece of 2mm thick acrylic board was obtained from SRC Physics Lab 2, and was laser cut into a 12mm diameter acrylic plate with 2.5mm diameter hole in the centre. Mabuchi RS-380PH-3270 motor was also obtained from the SRC Physics Lab 2, DC Power Supply were also borrowed from SRC Physics Lab 2. Red-dyed water was prepared by adding 10 drops of Star Brand Artificial Cochineal Red Colour food dye into 100ml of deionised (DI) water.

Green-dyed water with surfactants was prepared by mixing 10ml of Mama Lemon Hand soap with 90ml of DI water, before 10 drops of Star Brand Artificial Apple Green Colour was added into the mixture. Elro HL 400S Halogen Floodlight was borrowed from SRC Physics Lab 2 as light source and Samsung Galaxy S10 Plus smartphone was used as slow-motion camera.

### 3.2 Experimental Set-Up

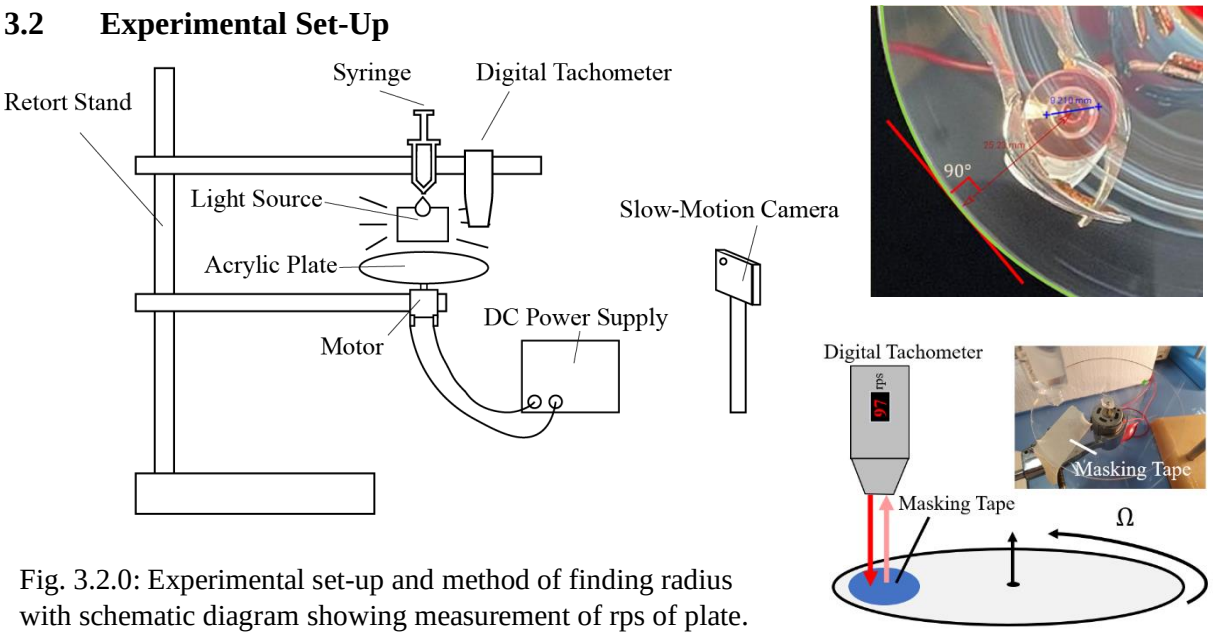


Fig. 3.2.0: Experimental set-up and method of finding radius with schematic diagram showing measurement of rps of plate.

The experiment was conducted in a dark room in a similar configuration as the one used by Povarov et al. (1976), with the only source of light being the floodlight shown in Fig. 3.2.0. The liquid droplet was released by a syringe containing either liquid, held vertically above the rotating plate and captured by a 960 fps slow-motion camera, while angular velocity (and hence surface speed) was varied using the DC power supply. A digital tachometer was used to record the rounds per second (rps) of the plate, and image of radius from where the drop lands to the centre of the plate was captured vertically below before tracker was used to measure it. Height of the syringe was varied using the clamp of the retort stand and was measured using a ruler.

### 3.3. Tracking

Motion Tracking (Fig 2.0) was done using OpenCV Python in the following order:

1. K-nearest neighbours background subtraction carried out on the original video, before image binarization and blurring.

2. Canny edge detection used to find the edges of the capsule.

3. Choose the largest detected contour to reduce noise in output

This allowed for better visualisation of the contour of the droplet and how it changes over time.

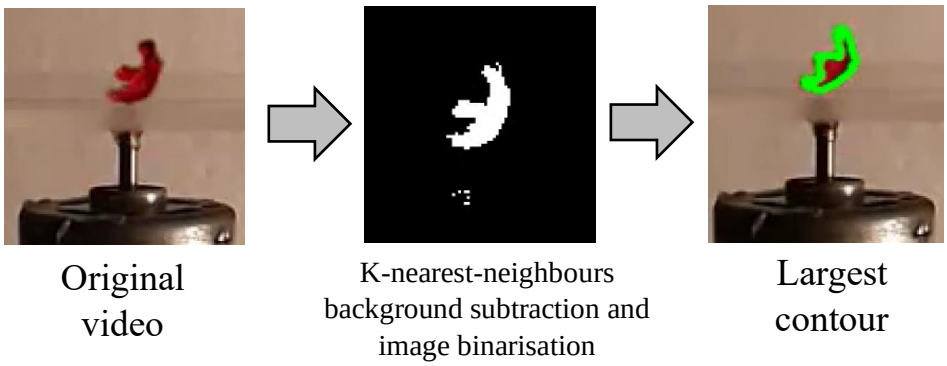


Fig. 3.3.0: Tracking of drop contour using Open CV in Python.

### 3.4. Motion of surrounding air


Fig. 3.4.0: Motion of surrounding fluids on the rotating plate.

Slow motion analysis of droplet moving in visible fluid or mist was conducted in order for better visualisation of the fluid dynamics surrounding the plate as the water drops onto it. A humidifier was used to generate mist onto the rotating plate, and a slow-motion camera was then used to capture the movement of the mist surrounding the plate. A water droplet was then dropped onto the rotating plate and the slow motion camera was used again to capture the dynamics of the mist as the water droplet landed on the plate (See Appendix A).

## 4. Theory and Characterisation

### 4.1. Theory

In experiments, it was observed that when the drop lands on the rotating plate, it will spread out, forming a circular disk. Conservation of energy can be used for modelling such a collision:

$$\frac{4\pi}{3}r^3\rho gh + 4\pi r^2\gamma_l = \pi R_{max}^2(\gamma_l + \gamma_{ls} - \gamma_s) + E_f \quad (1)$$

Substituting the Young and Dupre equation

$$\gamma_s = \gamma_{ls} + \gamma_l \cos\theta \quad (2)$$

Assuming $\theta = \pi$, an expression for $R$ can be obtained

$$R \leq \sqrt{\frac{2r^3\rho gh}{3\gamma_l} + 2r^2} \tag{3}$$

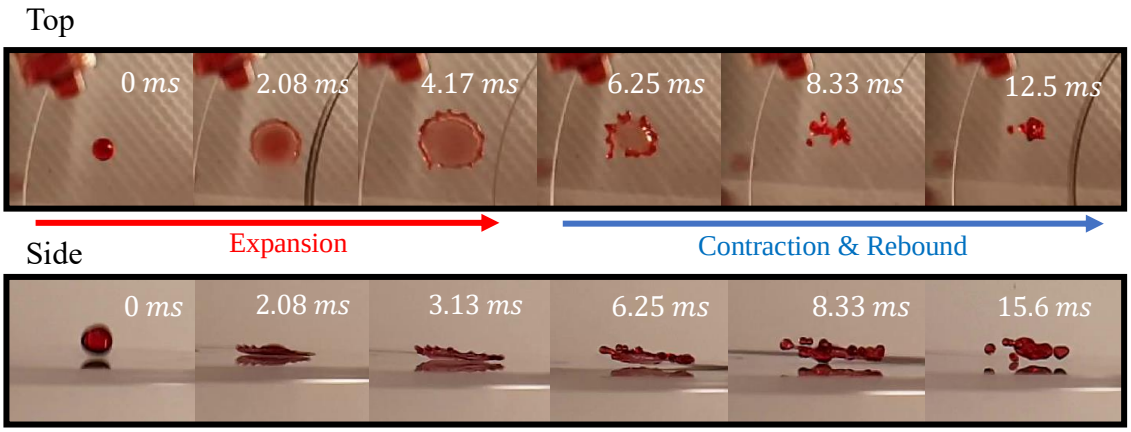


Fig. 4.1.0: Bouncing regime of droplet landing on moving surface (Top and side view)

The mean dynamic pressure, $p$ is proportional to $\rho_a v^2$, where $\rho_a$ is the density of air and $v$ is the speed of the plate (equal to speed of air close to the surface). The area of the drop is proportional to $R^2$. Hence, $F \propto \rho v^2 R^2$.

For the drop to rebound, $\int_0^T F\, dt = mv_i$.[2] By assuming constant force ($F$) throughout the collision and a constant collision time ($T$), the rebound condition is obtained:

$$\rho_a v^2 R^2 > \frac{m\sqrt{2gh}}{T} \tag{4}$$

## 4.2. Viscosity characterisation

Fig. 4.2.0: Spherical mass tracking.

A spherical mass was released with no initial velocity into a measuring cylinder with 120 ml of fluid. Its position is tracked and fitted using the following equation (See Appendix B)

$$m\ddot{z} = mg - 6\pi\mu Rv \tag{5}$$

| **Viscosity of dyed water ($m$ Pa $s^{-1}$)** | **Viscosity of water with surfactant ($m$ Pa $s^{-1}$)** |
|---|---|
| $0.602 \pm 0.1$ | $0.445 \pm 0.1$ |

[2] By Newton's Second Law, force is the rate of change of momentum. Hence, the integral of the minimum force needed is equal to the minimum change in momentum needed for rebound of the droplet. Hence, the rebounding velocity is calculated as 0 in this case.

## 4.3. Surface tension characterisation

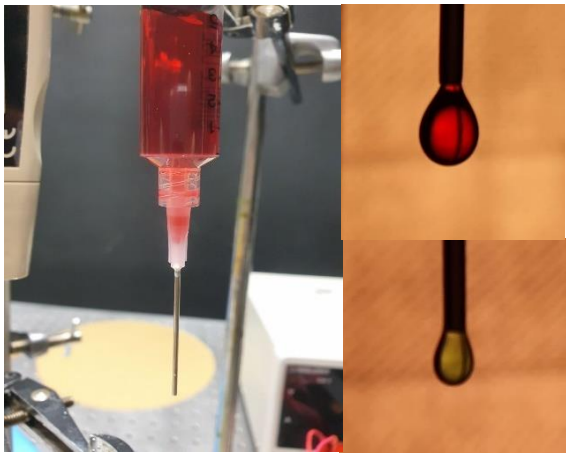

Fig. 4.3.0: Pendant drop method experiment set-up and image of pendant drop below a needle.

Surface tension has been characterised using the pendant drop method. In the pendant drop setup, a drop wass formed at the end of a needle as shown in the diagram. A pendant drop in equilibrium obeys the Young Laplace equation (See Appendix C):

$$\gamma\left(\frac{1}{R_1}+\frac{1}{R_2}\right)=\Delta P_0-\Delta\rho g z \tag{6}$$

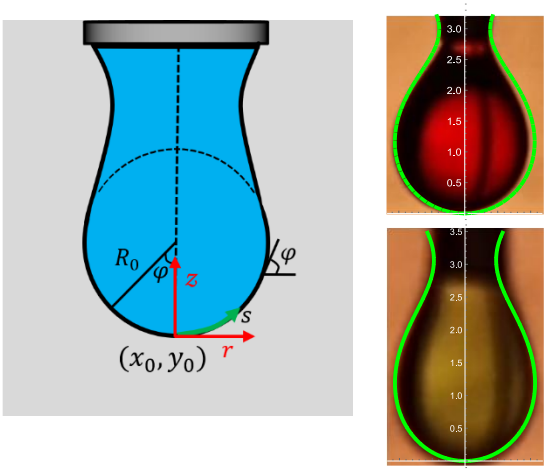


Fig. 4.3.1: Schematic diagram of pendant drop below a needle and graphs of droplet profile fitting using Mathematica.

This can be expressed in terms of cylindrical coordinates $r$ and $z$, together with the tangent angle $\varphi$. Hence, the Young Laplace equation can be obtained as a set of differential equations in terms of arc length $s$ measured from the drop's apex.

$$\begin{cases}\dfrac{d\varphi}{ds}=2-\dfrac{\Delta\rho g R_0^2}{\gamma}z-\dfrac{\sin\varphi}{r}\\ \dfrac{dr}{ds}=\cos\varphi\\ \dfrac{dz}{ds}=\sin\varphi\\ \varphi,r,z=0\ at\ z=0\end{cases} \tag{7}$$

| **Surface tension of water ($mN\ m^{-1}$)** | **Surface tension of water with surfactant ($\mathbf{m}N\ m^{-1}$)** |
|---|---|
| $83.5 \pm 9$ | $41.3 \pm 13$ |

## 5. Results and Discussion

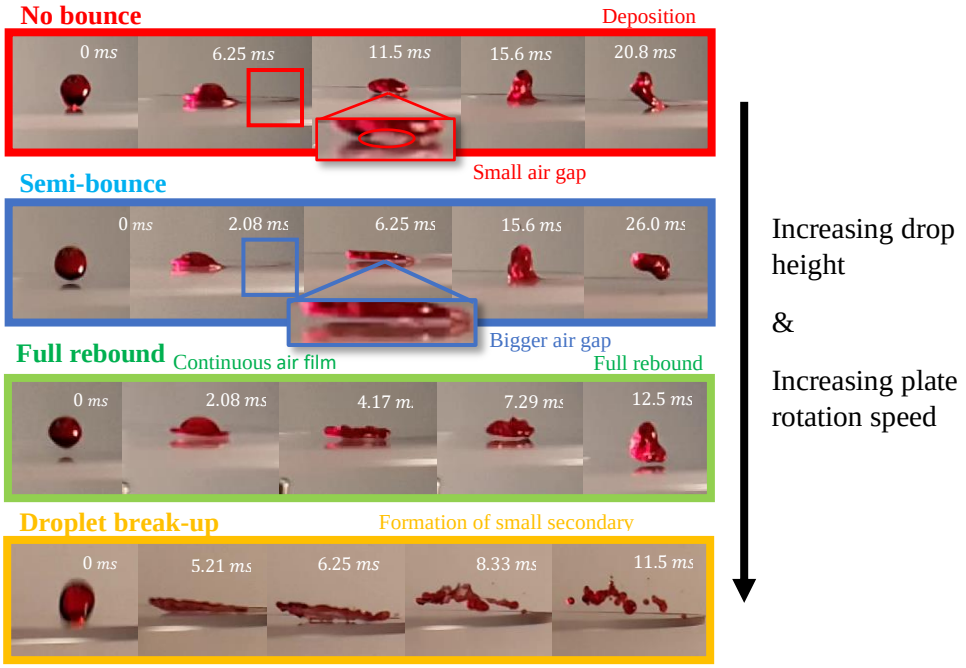


Fig. 5.1.0: 4 main regimes of drop interaction with rotating plate.

### 5.1. Phase Diagrams

From the experiments, 4 main regimes of the drop's interaction with the rotating plate were observed, namely: no bounce, semi-bounce, bounce, and break-up. As shown in Fig. 5.1.1, at low plate rotation speed($< 10\ m\ s^{-1}$), the drop either did not bounce, or partially bounced, due to the low air flow speed over the plate and hence a lower dynamic pressure ($\rho v^2$). The lift force generated was not sufficient to stop the droplet from sticking to the moving surface. At slightly higher plate speed ($10\sim15 m\ s^{-1}$), the drop might partially rebound. The drop first comes into contact with the plate. As the plate spins, it stretched the drop sideways and allows for an air film to be formed beneath it. Part of the drop adheres to the surface while the rest of the drop rebounds. At even higher plate speed ($20\sim40 m\ s^{-1}$), complete drop rebound was observed. At higher plate rotation speed, a continuous air film was formed beneath the drop, preventing it from adhering to the surface. The drop was then spread out over the air film, retracted, and rebounded. Increasing the plate speed even further would lead to the $4^{th}$ regime: droplet break-up. At such a high plate speed, the aerodynamic force from the moving air layer was strong enough that the surface tension force was unable to return the droplet to its spherical shape. The aerodynamic force then stretched the drop to a fine liquid circular sheet. The mode of break-up varied between drops and forming different structures before disintegrating into smaller droplets.

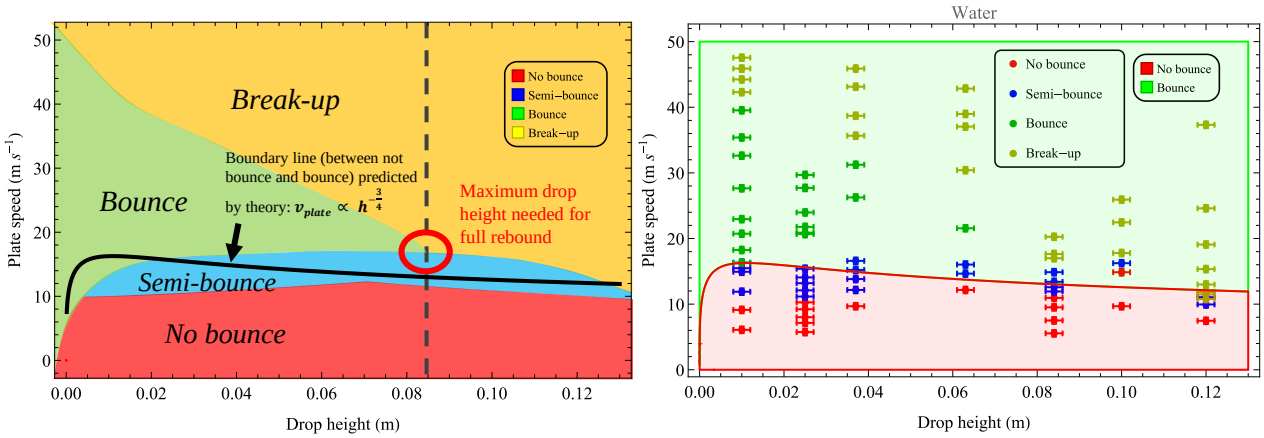


Fig. 5.1.1: Phase diagram showing theoretical boundary line (black) predicted by theory with actual values of 4 main regimes occurring in experiments for water (points)

For water with surfactant, a similar trend was observed as shown in Fig. 5.1.2. However, the boundaries between the different regimes were not as distinct as compared to normal water. This could be due to the reduced surface tension and viscosity of the liquid, resulting in the greater ease of drop break-up. The minimum plate speed required for complete rebound was also significantly lower at 10.5 $m\ s^{-1}$ as compared to 16.2 $m\ s^{-1}$ for normal water.

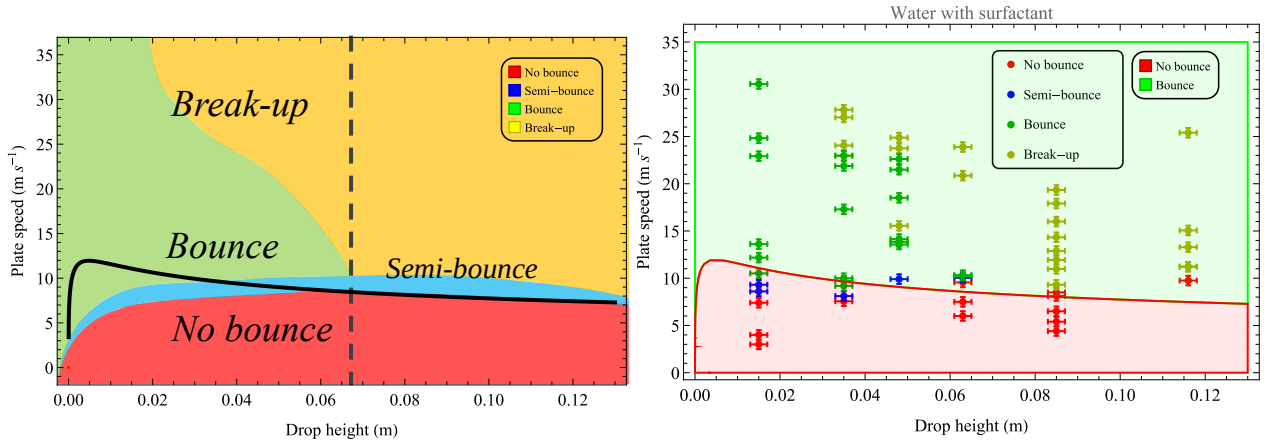


Fig. 5.1.2: Phase diagram showing theoretical boundary line predicted by theory (black) with actual values of 4 main regimes occurring in experiments for water with surfactant (points).

Moreover, it can be observed in Fig 8.1.1 that as the drop height increased (0.0475~0.085 $m$), the break-up and no bounce regimes are more dominant. At a higher height and hence impact velocity, the kinetic energy of the droplet increased and more energy was converted to the surface free energy of the water droplet until it was unable to sustain a stable shape, resulting in formation of secondary droplets. The maximum drop height ($h_{crit}$) where full rebound was observed is 0.625$m$. Beyond this critical value, no full rebound was observed.

For water with surfactant, a similar trend was observed. At At low height, the break-up regime was not observed unlike that for water. This could be due to its smaller drop size due to lower surface tension, thus making it harder for the aerodynamic force to perturb its surface, leading to less break-up. In contrast, at high height ($> 0.65\,m$), the minimum plate speed at which break-up regime occurs for water with surfactant was much lower ($10\,m\,s^{-1}$) as compared to water ($16\,m\,s^{-1}$). It can be concluded that gravity has a more significant effect than the plate speed on the break- up of smaller drops as compared to bigger drops. Even though $h_{crit}$ for water with surfactant remains roughly constant, the plate speed at which it occurs is drastically different at $11\,m\,s^{-1}$ as compared to $22\,m\,s^{-1}$ for water. This could be due to the reduced surface tension and viscosity of the liquid, resulting in the greater ease of drop break-up.

## 5.2. Modes of droplet break-up

The most seen mode of droplet break-up is shown in Fig. 5.2.0.

During the impact, a radially spreading lamella is formed. At high impact velocity, the lamella is radially ejected at an inclination angle with respect to the rotating plate. This is typically known as "crown splash". As the lamella continues to expand and stretch, the rim gradually becomes more unstable, eventually disintegrating into secondary droplets.

*Crown Splash*

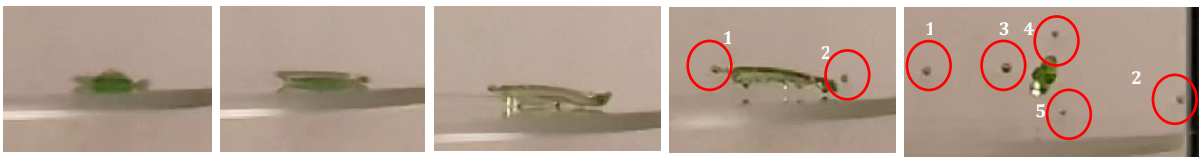


Fig. 5.2.0: Image showing "crown splash", the most common mode of droplet break-up observed.

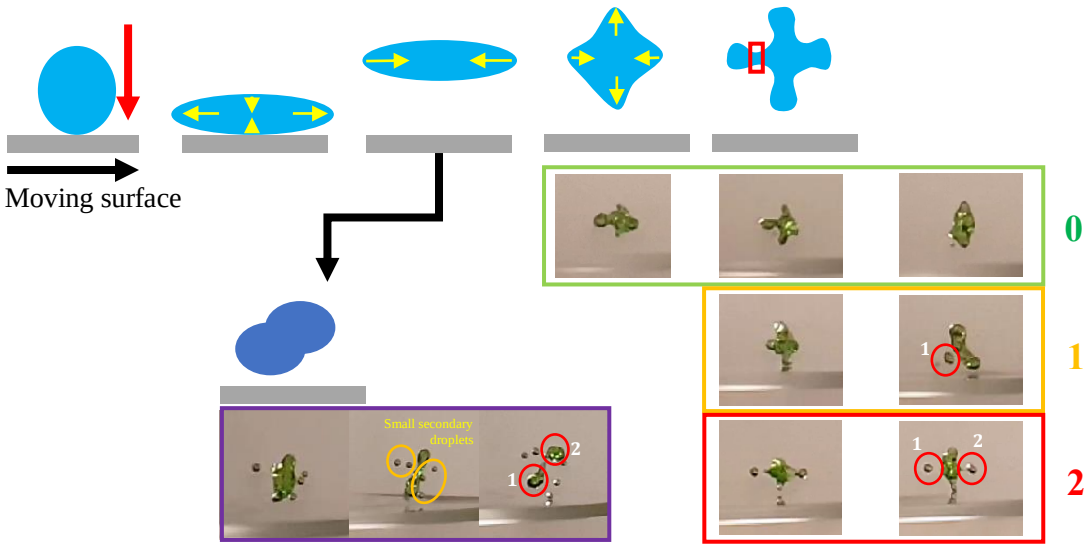


Fig. 5.2.1: Diagram showing the other modes of droplet break-up

Other modes of break-up which have not been reported by other research papers were also observed. Upon impact, the drop compresses and turns into an oblate spheroid. The surface tension force acts as a restoring force to turn the shape of a drop back to a sphere, which is the most stable shape it can attain. The 2 ends of the oblate spheroid then pushes inwards along the semi major axis. By conservation of volume, the drop is pushed outwards along the semi-minor axis. This results in a resulting star-shape. However, this star-shape is highly unstable and may disintegrate into smaller, secondary droplets which are more stable. In experiments, such a star shape was observed to produce up to 2 secondary droplets. The number of secondary droplets increases as the plate speed and impact velocity increases due to the greater aerodynamic force and greater perturbation to the geometry of the drop.

Occasionally, the drop was also observed to be splitting into 2 relatively big drops in the diagonal direction. The drop rotates as it rebounds due to the moving air layer beneath it which results in a rotational shear force. This rotation creates centrifugal force on the surface fluids elements, pushing them outwards and away from the centre of the drop. When the centrifugal force overcomes the surface tension, the drop breaks up.

## 5. Conclusion and Recommendations for future work

In conclusion, the regime of water dropping onto a moving surface was analysed in detail and supported with phase diagrams and high-speed footage of the drop in this paper. The different modes of water break up at high surface and impact velocity were explored. It was found that surface velocity, impact velocity, liquid viscosity and surface tension were all able to affect the dynamics of water bouncing off a moving surface. There is also a qualitative agreement between theory and experiment. The unique phenomena has many applications in real world situations, such as in inkjet printers. This research would for the optimisation of speed of paper in industrial printers to prevent unwanted splashing and smudging of ink droplets. It is also applicable for optimising and preventing aircraft icing, etc.

However, the surface material and angle was not varied and changed due to limitations of the materials available. The ambient conditions such as surrounding air and temperature also remained constant and were not varied. Hence, there is potential for more future work to be done in these areas. Modelling of the droplet hitting the plate was also attempted using computational fluid dynamics, however, due to limited expertise in this area, computational

fluid dynamics were unable to provide much insight into the regime of water bouncing off a moving surface. Thus, there can also be more potential future work to be done in this area.

**Acknowledgements**

We would like to thank Mdm Foo and Mdm Chua of the SRC Lab staff for being kind enough to provide their attention to our project, and for their invaluable contributions and help to it. We would also like to thank our school's SRC labs for providing all necessary materials to conduct the experiments required. We would also like to thank Mr Fong, our mentor, without which this project would not have come to fruition, for his priceless insights and efforts towards making this project as successful as possible.

**References**

Bird, J., Dhiman, R., Kwon, H., & Varanasi, K. (2013). Reducing the contact time of a bouncing drop. *Nature*, *503*(7476), 385-388. doi: 10.1038/nature12740

Bragg, M. (1996). Aircraft aerodynamic effects due to large droplet ice accretions. *34Th Aerospace Sciences Meeting And Exhibit*. doi: 10.2514/6.1996-932

Bouwhuis, W. (2015). *Dynamics of deforming drops*.

Chubynsky, M., Belousov, K., Lockerby, D., & Sprittles, J. (2020). Bouncing off the Walls: The Influence of Gas-Kinetic and van der Waals Effects in Drop Impact. *Physical Review Letters*, *124*(8). doi: 10.1103/physrevlett.124.084501

Gauthier, A., Bouillant, A., Clanet, C., & Quéré, D. (2018). Aerodynamic repellency of impacting liquids. Physical Review Fluids, 3(5). doi: 10.1103/physrevfluids.3.054002

Kolinski, J., Mahadevan, L., & Rubinstein, S. (2014). Lift-Off Instability During the Impact of a Drop on a Solid Surface. *Physical Review Letters*, *112*(13). doi: 10.1103/physrevlett.112.134501

Lhuissier, H., Tagawa, Y., Tran, T., & Sun, C. (2013). Levitation of a drop over a moving surface. Journal Of Fluid Mechanics, 733. doi: 10.1017/jfm.2013.470

Moghtadernejad, S., Lee, C., & Jadidi, M. (2020). An Introduction of Droplet Impact Dynamics to Engineering Students. *Fluids*, *5*(3), 107. doi: 10.3390/fluids5030107

Povarov, O., Nazarov, O., Ignat'evskaya, L., & Nikol'skii, A. (1976). Interaction of drops with boundary layer on rotating surface. Journal Of Engineering Physics, 31(6), 1453-1456. doi: 10.1007/bf00860580

Roisman, I. (2009). Inertia dominated drop collisions. II. An analytical solution of the Navier–Stokes equations for a spreading viscous film. *Physics Of Fluids*, *21*(5), 052104. doi: 10.1063/1.3129283

Sawaguchi, E., Matsuda, A., Hama, K., Saito, M., & Tagawa, Y. (2019). Droplet levitation over a moving wall with a steady air film. *Journal Of Fluid Mechanics*, *862*, 261-282. doi: 10.1017/jfm.2018.952

Son, H., Lee, S., & Lee, J. (2020). Numerical Analysis of Drag Force Acting on 2D Cylinder Immersed in Accelerated Flow. *Water*, *12*(6), 1790. doi: 10.3390/w12061790

Wu, Z. (2018). Drop "impact" on an airfoil surface. *Advances In Colloid And Interface Science*, *256*, 23-47. doi: 10.1016/j.cis.2018.05.005

## Appendices

### Appendix A. Modelling air flow over circular plate (Von Karmon swirling flow)

The velocity of the air could be written (in cylindrical coordinates) as:

$$\mathbf{v}(\mathrm{r},\mathrm{z}) = \mathrm{u}(\mathrm{r},\mathrm{z})\ \mathbf{e}_{\mathrm{r}} + \mathrm{v}(\mathrm{r},\mathrm{z})\ \mathbf{e}_{\theta} + \mathrm{w}(\mathrm{r},\mathrm{z})\mathbf{e}_{\mathrm{z}}$$

Where $\mathbf{e_r}$, $\mathbf{e_\theta}$ and $\mathbf{e_z}$ are unit vectors in cylindrical coordinates.

The Navier- Stokes equation reduce to:

$$\begin{cases} \frac{1}{r}\frac{\partial}{\partial r}(\mathrm{r\ u}) + \frac{\partial w}{\partial z} = 0 \\ u\frac{\partial \mathrm{u}}{\partial \mathrm{r}} + w\frac{\partial u}{\partial z} - \frac{v^2}{r} = -\frac{1}{\rho}\frac{\partial p}{\partial r} + \nu\left(\frac{\partial^2 u}{\partial r^2} + \frac{1}{r}\frac{\partial u}{\partial r} + \frac{\partial^2 u}{\partial z^2} - \frac{u}{r^2}\right) \\ u\frac{\partial v}{\partial r} + w\frac{\partial v}{\partial z} + \frac{vu}{r} = \nu\left(\frac{\partial^2 v}{\partial r^2} + \frac{1}{r}\frac{\partial v}{\partial r} + \frac{\partial^2 v}{\partial z^2} - \frac{v}{r^2}\right) \\ u\frac{\partial w}{\partial r} + w\frac{\partial w}{\partial z} = \frac{-1}{\rho}\frac{\partial p}{\partial z} + \nu(\frac{\partial^2 w}{\partial r^2} + \frac{1}{r}\frac{\partial w}{\partial r} + \frac{\partial^2 w}{\partial z^2}) \end{cases}$$

Boundary conditions:

$$\begin{cases} \vec{\mathbf{u}}_{\mathbf{r}}(\mathrm{r},0) = 0 \\ \vec{\mathbf{u}}_{\boldsymbol{\theta}}(\mathrm{r},0) = \Omega \\ \vec{\mathbf{u}}_{\mathbf{z}}(\mathrm{r},0) = 0 \\ \vec{\mathbf{u}}_{\mathbf{r}}(\mathrm{r},\infty) = 0 \\ \vec{\mathbf{u}}_{\boldsymbol{\theta}}(\mathrm{r},\infty) = 0 \end{cases}$$

The images below are the simulation results done using ANSYS FLUENT. Due to time constraint, the droplet was not incorporated in the simulation.

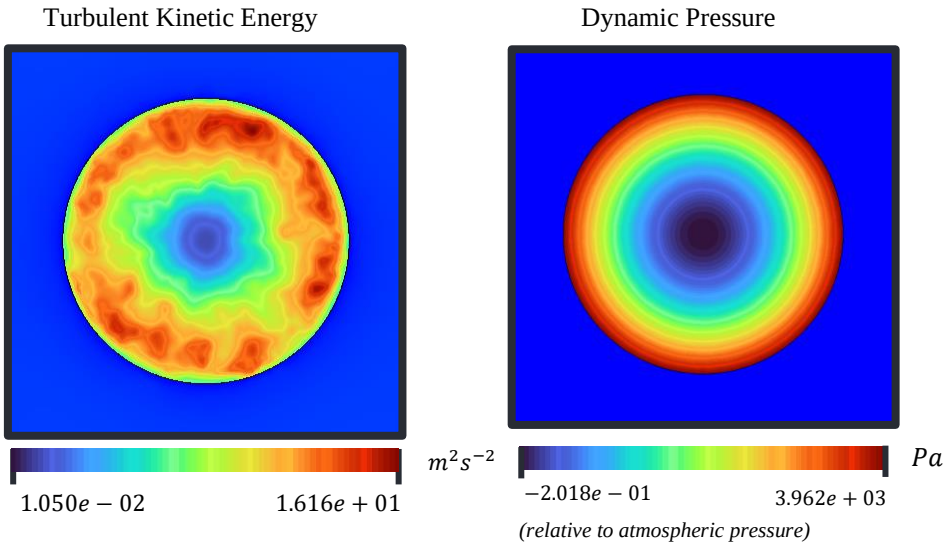


**Appendix B. Stoke's Viscosity Law**

$$m\ddot{z} = mg - 6\pi\mu Rv$$

This is the equation of motion of a spherical mass in a liquid with dynamic viscosity $\mu$.

The following equation is obtained after solving the equations of motion:

$$z(t) = \frac{e^{-\frac{6\pi Rt\mu}{m}} mg\left(m - \left(m + 6e^{\frac{6\pi Rt\mu}{m}}\pi Rt\mu\right)e^{\frac{6\pi Rt\mu}{m}}\right)}{36(\pi R\mu)^2}$$

**Appendix C. Pendant drop method for characterisation of surface tension**

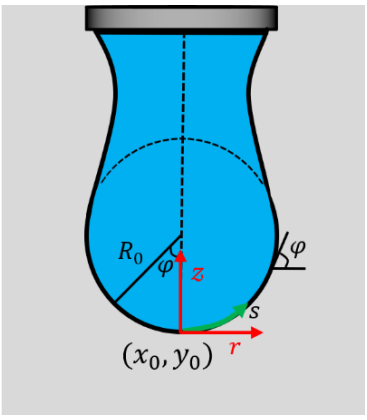


In the pendant drop method, the Young-Laplace equation can be expressed as a set of differential equations:

$$\begin{cases} \dfrac{d\varphi}{ds} = 2 - \dfrac{\Delta\rho g R_0^2}{\gamma} z - \dfrac{\sin\varphi}{r} \\ \dfrac{dr}{ds} = \cos\varphi \\ \dfrac{dz}{ds} = \sin\varphi \\ \varphi, r, z = 0 \ at \ z = 0 \end{cases}$$

Where cylindrical coordinates $\varphi, r, z$ is as defined in the figure on the left, $\Delta\rho$ is the density difference between the water and surrounding air, $R_0$is defined as the radius of water droplet.